water

MDPI

Article

Spatio-Temporal Characteristics of Land Subsidence and Driving Factors Analysis in Shenzhen

Shuanglong Wang [1], Guoyang Wang [2,3,*], Min Huang [1], Jun Song [1], Xiaoyu Yang [1], Tingyu Zhang [1], Wenyu Ji [2,3], Shuai Zhang [1], Weili Wu [2], Chengwen Wei [1] and Jian Xiao [1]

[1] Shenzhen Intergrated Geotechnical Investigation & Surveying Co., Ltd., Shenzhen 518000, China; wsloon@gmail.com (S.W.); chidaoxue100@163.com (M.H.); 13510174800@139.com (J.S.); gxm46zykk4@gmail.com (X.Y.); tingyuzhang1999@126.com (T.Z.); zhangshuai5337@gmail.com (S.Z.); chengwen2046@126.com (C.W.); 18126293900@163.com (J.X.)
[2] Institute of Estuarine and Coastal Zone, College of Marine Geosciences, Key Lab of Submarine Geosciences and Prospecting Technology, Ministry of Education, Ocean University of China, Qingdao 266100, China; jiwenyu@stu.ouc.edu.cn (W.J.); 13858319531@163.com (W.W.)
[3] Laboratory of Marine Geology, Qingdao National Laboratory for Marine Science and Technology, Qingdao 266061, China
* Correspondence: wangguoyang@ouc.edu.cn; Tel.: +86-185-6159-7517

Abstract: Analyzing land subsidence using Multi-temporal Interferometric Synthetic Aperture Radar (MT-InSAR) technology holds significant importance for the secure development of urban areas. Shenzhen, being a crucial component of the Pearl River Delta, faces the threat of land subsidence, similar to most deltaic cities. Numerous studies have already indicated the presence of severe land subsidence in certain localities of Shenzhen. However, due to limitations in data scope and research methodologies, the comprehensive spatial-temporal distribution of land subsidence across the entire city of Shenzhen remains unclear. This study initially employed MT-InSAR technology to process a total of 534 Sentinel-1A SAR images from three different frames (P11F71, P113F71, P11F65), covering the entire city of Shenzhen. This processing resulted in the generation of subsidence rate maps and subsidence time series. Subsequently, the temporal evolution patterns of the subsidence were analyzed while significant subsidence regions were identified. By integrating information from optical images reflecting human activities on the Earth's surface, the study deduced the subsidence mechanisms in various significant subsidence areas. Research findings indicate that land subsidence in Shenzhen is primarily caused by construction activities, with a concentration in the western coastal areas of Shenzhen, reaching a maximum rate of 80 mm/yr, located at the estuary of Dongbao River (113.770385, 22.745305). The cumulative subsidence from March 2017 to June 2023 amounts to 500 mm. The expansion of the Qinglinjing Reservoir has led to an increased demand for water, resulting in a significant rise in formation pressure and subsequent land subsidence. InSAR land subsidence monitoring and analysis in urban areas can address the spatial and temporal resolution limitations of traditional subsidence monitoring methods, providing effective recommendations for widespread subsidence prevention and control.

Keywords: Multi-Temporal InSAR; driving factors analysis; construction-induced subsidence; coastal subsidence; reservoir-induced subsidence

Citation: Wang, S.; Wang, G.; Huang, M.; Song, J.; Yang, X.; Zhang, T.; Ji, W.; Zhang, S.; Wu, W.; Wei, C.; et al. Spatio-Temporal Characteristics of Land Subsidence and Driving Factors Analysis in Shenzhen. *Water* **2024**, *16*, 1200. https://doi.org/10.3390/w16091200

Academic Editor: Alessandro Bergamasco

Received: 19 March 2024
Revised: 9 April 2024
Accepted: 17 April 2024
Published: 23 April 2024

1. Introduction

Estuarine and coastal zones often experience high population density and possess significant economic value [1]. However, due to the combined influence of human and natural factors, these estuarine areas are frequently prone to disasters [2,3]. Among various disasters, land subsidence is a relatively concealed yet highly destructive geological hazard [4]. Land subsidence poses challenges to the safety of human lives and property, as well as the management of social order, creating obstacles for urban sustainable development [1,3,5–7].

Therefore, the monitoring and analysis of land subsidence hold significant importance for its prevention and control.

According to previous studies, coastal subsidence can, on one hand, lead to the sinking and cracking of engineering structures such as embankments and drainage stations [8,9], resulting in a reduction in the coastal area's flood control, drainage, and tide prevention capabilities. On the other hand, it can significantly contribute to the local relative sea-level rise [10–12], thereby exacerbating the risk of coastal flooding [12,13], soil salinization, shoreline retreat, and wetland degradation [11,14]. This, in turn, diminishes the coastal area's capacity to withstand threats from the ocean, presenting more severe challenges to human safety and environmental protection in coastal regions [2–4,6,14]. Compared to the global absolute sea-level rise, land subsidence may exert adverse effects on coastal flood risks that are ten times greater or more [15,16]. Moreover, even if the probability of coastal flooding is not increased by constructing protective facilities, the combined influence of land subsidence and sea-level rise is projected to raise global flood losses to a range of $60 to $63 billion annually by 2050 [17].

Regions in China, including the Yangtze River Delta [18], the Yellow River Delta [19–21], the Pearl River Delta [22,23], and North China Plain [24,25], are currently experiencing high rates of subsidence due to the combined influence of natural factors and human activities. Taking the research area of Shenzhen as an example: Xu, Feng [26] conducted a detailed analysis using the Small Baseline Subset (SBAS) Interferometric Synthetic Aperture Radar (InSAR) technique to investigate the land subsidence rates in the land reclamation areas of western Shenzhen. The study revealed a significant trend of land subsidence in this region, particularly evident around Shenzhen Airport, Bao'an Center, Qianhai Bay, and Shenzhen Bay. The subsidence rates reached up to 25 mm/year, and it is anticipated that subsidence will persist in the near future [26]. Du, Feng [27] employed Permanent Scatterers (PS) InSAR technology and multi-source SAR data to extract land subsidence rates in the coastal areas of western Shenzhen. Their findings revealed uneven land subsidence in this region. Building upon previous research, Liu, Chen [28] summarized the progress in subsidence studies in the western coastal areas of Shenzhen. They observed that land reclamation projects and the construction of metro systems in this region have, to a certain extent, accelerated the land subsidence [28]. Sun, Du [29], integrating data on coastal reclamation, transportation networks, and urban development, analyzed the relationship between land subsidence and the urbanization process. They similarly identified land subsidence in the coastal areas and metro construction zones in western Shenzhen. Zhou, Liu [30] were the first to discover land subsidence near the Qinglinjing Reservoir in Shenzhen. They combined geological expertise to analyze the causative factors, attributing them to the engineering geological conditions in the area.

In summary, the current body of studies predominantly focus on land subsidence in the western coastal areas of Shenzhen [26], including subsidence associated with metro construction [31]. Additionally, some studies concentrate on algorithmic innovations [32–34] and flood risk analysis [23,35]. Consequently, there is a current lack of comprehensive studies covering the overall and integrated land subsidence status across the entirety of Shenzhen.

Moreover, as evident from the aforementioned studies, Multi-Temporal InSAR (MT-InSAR) technology has been widely employed in the monitoring of land subsidence in Shenzhen. MT-InSAR technology offers high spatio-temporal resolution, enabling extensive and long-term studies with fine spatial resolution. This has elevated researchers' understanding of land subsidence to a new level. The advent of InSAR technology and the continuous updating of satellite data have had a groundbreaking impact on studying subsidence patterns and spatial expansion trends. However, the in-depth analysis of InSAR data results in the above studies is not comprehensive enough, particularly in terms of insufficient time-series analysis. Furthermore, there is a lack of land subsidence results covering the entire city of Shenzhen.

Therefore, this study will utilize MT-InSAR technology to first conduct monitoring and analysis in the research area. Subsequently, in conjunction with machine learning algorithms, the study will classify and analyze land subsidence in Shenzhen based on spatiotemporal patterns, identifying driving factors. The goal is to provide a high-precision assessment of land subsidence in Shenzhen and contribute valuable insights to support urban sustainable development.

2. Study Area

Shenzhen, as illustrated in Figure 1b, exhibits a complex geological and geomorphic landscape, characterized by its sensitive natural environment. The intricate and fragile geographical conditions in this region have historically led to frequent natural disasters. Over the past four decades of China's reform and opening-up, Shenzhen has experienced rapid economic development, ranking first in population density nationwide. Extensive human activities, such as construction projects and the development and utilization of underground resources, have significantly altered the original topographic and structural characteristics of the region, as well as disturbed the balance of geostress. Consequently, the land subsidence hazard in the Shenzhen area has become increasingly severe.

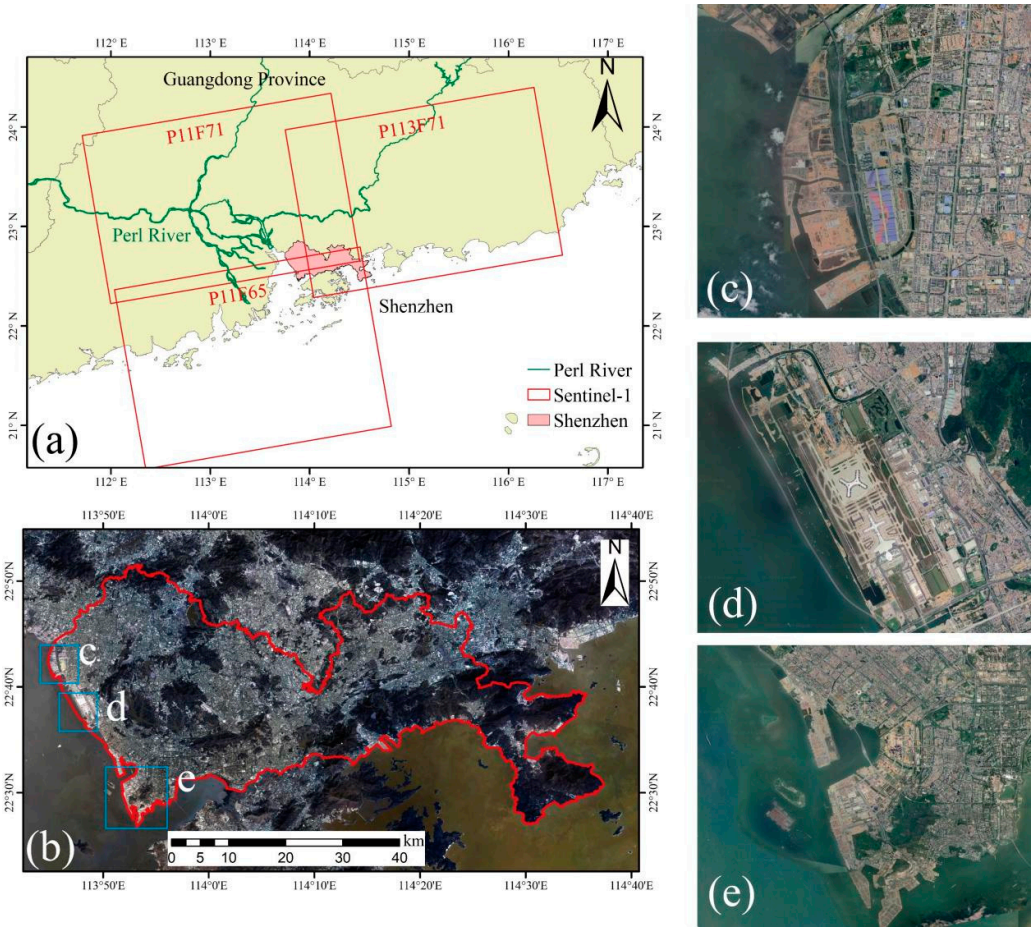

Figure 1. Study area. (**a**) Coverage of Sentinel-1 data, (**b**) Coverage of the study area (Landsat-8, https://earthexplorer.usgs.gov/, accessed on 3 October 2023), (**c**–**e**) representative the reclamation areas (Google Earth, https://earth.google.com/, accessed on 3 October 2023).

The city of Shenzhen has an elongated shape, stretching from east to west, with a narrow width in the north–south direction, covering a total area of 1953 km^2. The highest peak in Shenzhen is Wutong Mountain, with an altitude of 943.7 m, while the average altitude of the entire city is approximately 81 m. The predominant landforms include hills

and plains, with hills above 100 m in elevation occupying 48.89% of the land area and plains covering 49.56%, while the remaining portion consists of water bodies. Positioned as a burgeoning city along the coastline, Shenzhen boasts a coastline of 257 km and a maritime area of 1145 km^2. It features three bays and an estuary, namely Dapeng Bay, Daya Bay, Shenzhen Bay, and the Pearl River Estuary, establishing itself as a truly significant marine metropolis. With excellent deep-water channels, the eastern ports of Shenzhen rank among the world's busiest container ports.

However, when faced with the extensive reclamation illustrated in Figure 1c–e and the construction of numerous surface buildings, bridges, underground tunnels, deep foundation projects, and metro constructions in the context of complex geological formations, the gradual consolidation of reclaimed areas and the sustained effects of the loads from surface structures inevitably lead to land subsidence. This occurrence is not only unavoidable but also poses a threat to urban development and the safety of human lives and property. Therefore, it is of significant practical importance to promptly understand the land subsidence situation in the reclamation areas of Shenzhen after the completion of land reclamation projects.

3. Material and Methods

3.1. Datasets

The MT-InSAR computations in this study utilized Sentinel-1 data. Since the Sentinel-1B satellite has been decommissioned with no new data updates, this research primarily relied on ascending orbit data from Sentinel-1A. Additionally, as a single frame does not cover the entire area of Shenzhen, this paper processed data from three frames: Path113 Frame71, Path11 Frame71, and Path11 Frame65. The spatial coverage of these frames is illustrated in Figure 1a.

The data information involved in the calculations is presented in Table 1.

Table 1. Detailed information of the Sentinel data in the computations.

	Interferometric Processing Coverage	**Temporal Analysis Coverage**
P11F71	12 March 2017–13 September 2023 (190)	20 September 2017–9 June 2023 (169)
P113F71	27 September 2017–27 August 2023 (184)	27 September 2017–16 June 2023 (156)
P11F65	12 March 2017–9 June 2023 (160)	20 September 2017–9 June 2023 (146)

Additionally, the obtained datasets include SRTM-30 data and ERA5 data. The SRTM data is utilized for topographic phase removal in InSAR data processing, while ERA5 data is employed for atmospheric correction in interferogram processing.

3.2. MT-InSAR

The Small Baseline Subset (SBAS) algorithm is characterized by relatively short temporal and spatial baselines, which effectively avoids the decorrelation effects introduced by excessively long baselines and enhances the constraint on the data [36]. Based on specific thresholds for temporal and spatial baselines, interferograms can be grouped into several sets, where the interferograms within each set have sufficiently short and coherent baselines. This ensures high coherence and more accurate estimation of atmospheric and DEM errors, thereby effectively improving the precision of time-series analysis. To effectively invert surface deformation, all interferogram sets are generally selected, but the solution matrix formed between these sets is typically singular. To address this issue, singular value decomposition (SVD) is commonly employed to obtain the minimum norm solution or the least squares solution for the inversion matrix.

In this section, three sets of data were individually subjected to interferometric processing and time-series analysis, the data processing flowchart is shown in the Figure 2. The results were then integrated to form a comprehensive depiction of land subsidence across the entire city of Shenzhen. The time baselines for the three datasets are generally within 36

days, and the maximum spatial baseline does not exceed 330 m. Multi-looking processing was applied during the interferometric processing to enhance the signal-to-noise ratio. A total of 502, 477, and 471 interferograms were obtained for each dataset. The spatiotemporal baselines of the interferograms are illustrated in Figure 3.

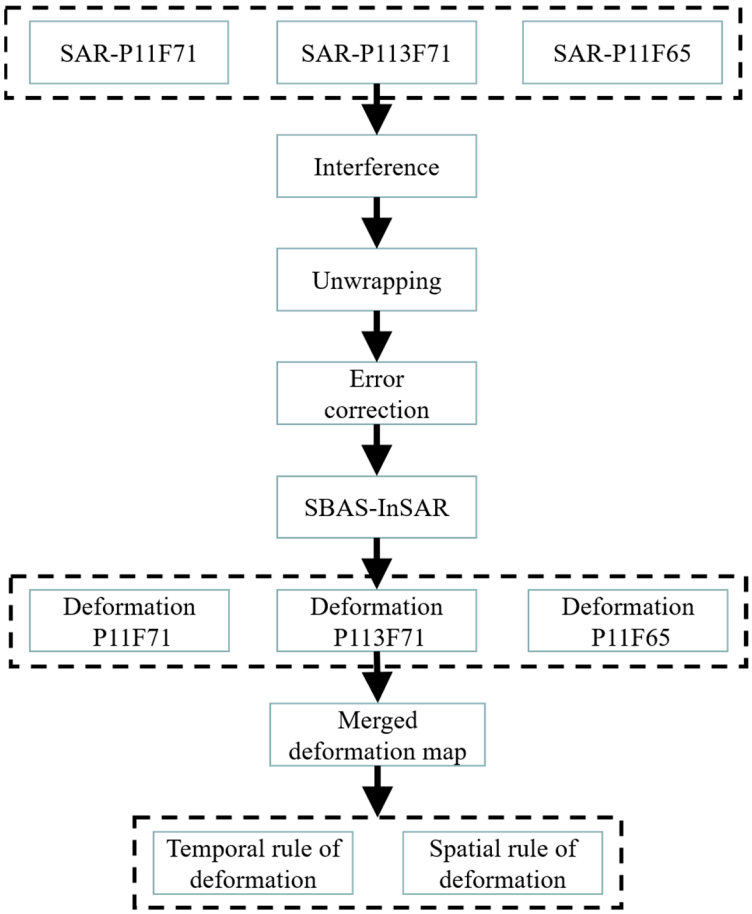

Figure 2. Flowchart of data process.

During interferometric processing, we generated as many interferograms as possible to ensure data redundancy. However, to maintain consistent temporal coverage for the final time-series analysis, the time range of interferograms used in the analysis is outlined in Table 2.

Table 2. Some key parameters in the interferometric processing are presented as following.

Parameters	P11F71	P113F71	P11F65
Temporal baseline	12–60 days	12–84 days	12–144 days
The max perpendicular baseline	1–321 m	1–336 m	1–328 m
Unwrapping coherence threshold	0.4	0.4	0.4
Multi-looking	20 × 5	20 × 5	20 × 5
Unwrapping method	MCF	MCF	MCF
DEM and resolution	SRTM 30 m with height datum of WGS84	SRTM 30 m with height datum of WGS84	SRTM 30 m with height datum of WGS84
Precise orbital data	Yes	Yes	Yes
Filter method	Gaussian filter	Gaussian filter	Gaussian filter
Number of interferograms	502	477	471
Orbital Ramp Remove	YES	YES	YES
Atmospheric correction	ERA5	ERA5	ERA5

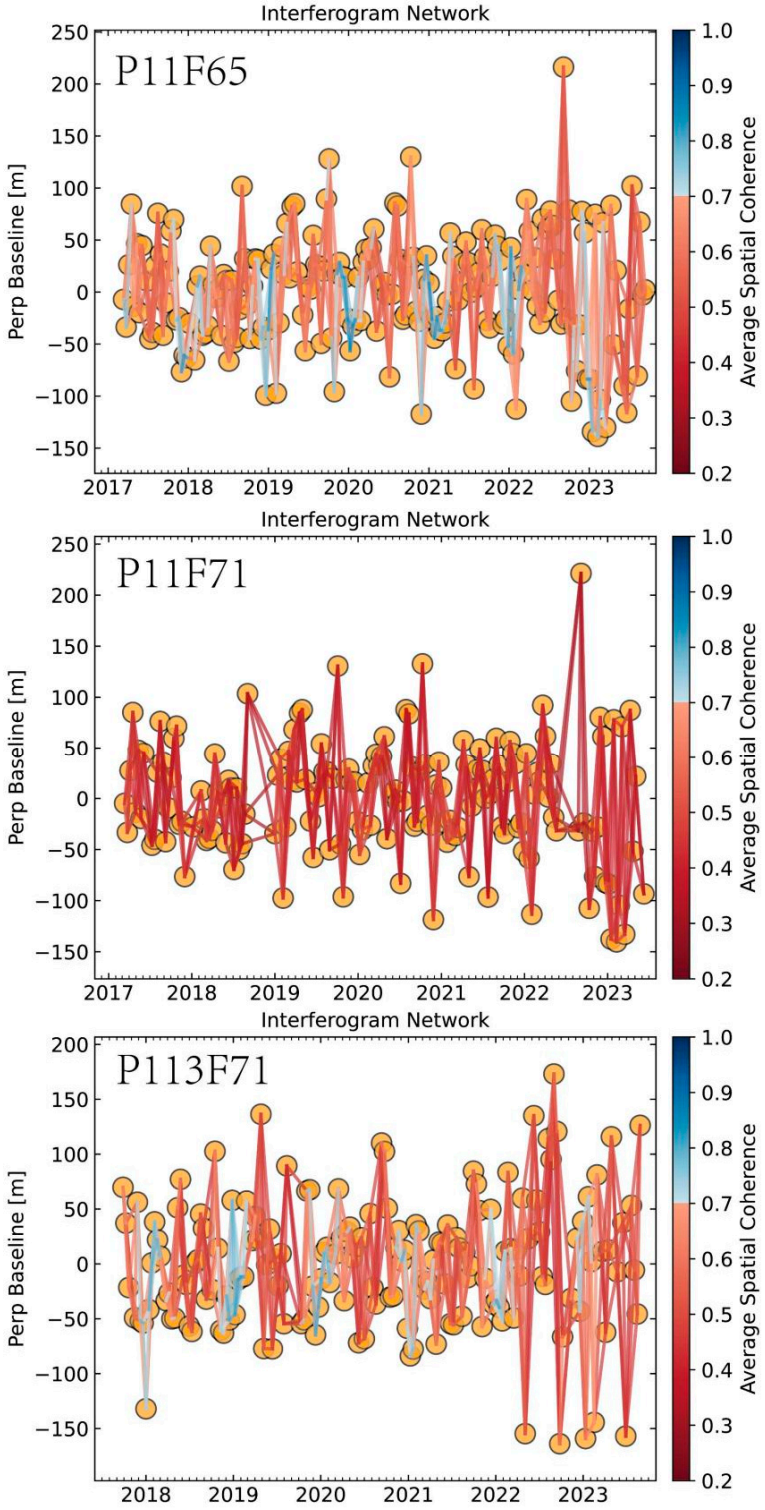

Figure 3. Spatial-temporal baseline plot.

3.3. The Merging of Subsidence Rate Maps

Since the three Frames covering the study area are processed separately, merging the results is necessary to obtain a complete deformation profile of the study area. The merging principle relies on averaging the differences of coherent targets' common points within the overlapping areas [37]. In this study, the main reference for merging is the common points in the overlapping areas of the three different Frames, with P11F71 serving as the master image. The differences between P11F65 and P11F71, as well as between P113F71

and P11F71, are calculated within the overlapping areas and then applied as correction values. The reference offset between adjacent orbits can be calculated using the following two formulas (1) and (2).

$$\Delta v_{off} = \frac{\sum_{i=0}^{i=N-1}(v_{mi} - v_{si})}{N} \quad (1)$$

$$v'_{si} = v_{si} + \Delta v_{off} \quad (2)$$

Δv_{off} represents the reference offset between adjacent orbits, v_{mi} is the deformation rate of coherent targets in the master reference Frame; v_{si} is the deformation rate of coherent targets in the slave frame to be corrected; v'_{si} is the deformation rate of the slave image corrected based on the calculated offset. N represents the number of common points.

4. Results

4.1. Land Subsidence Rate Map

After conducting MT-InSAR analysis of land subsidence in the study area, the vertical subsidence rate map shown in Figure 4 is obtained. From the map, it can be observed that apart from the coastal areas and the Qinglinjing Reservoir, where significant subsidence is evident, the majority of the region remains relatively stable. However, there are numerous dispersed small-scale subsidence centers within the urban area. Therefore, the surface subsidence in the Shenzhen region can be roughly categorized into three types: concentrated subsidence distribution in coastal reclamation areas, concentrated subsidence in the Qinglinjing Reservoir area, and scattered subsidence throughout the entire region.

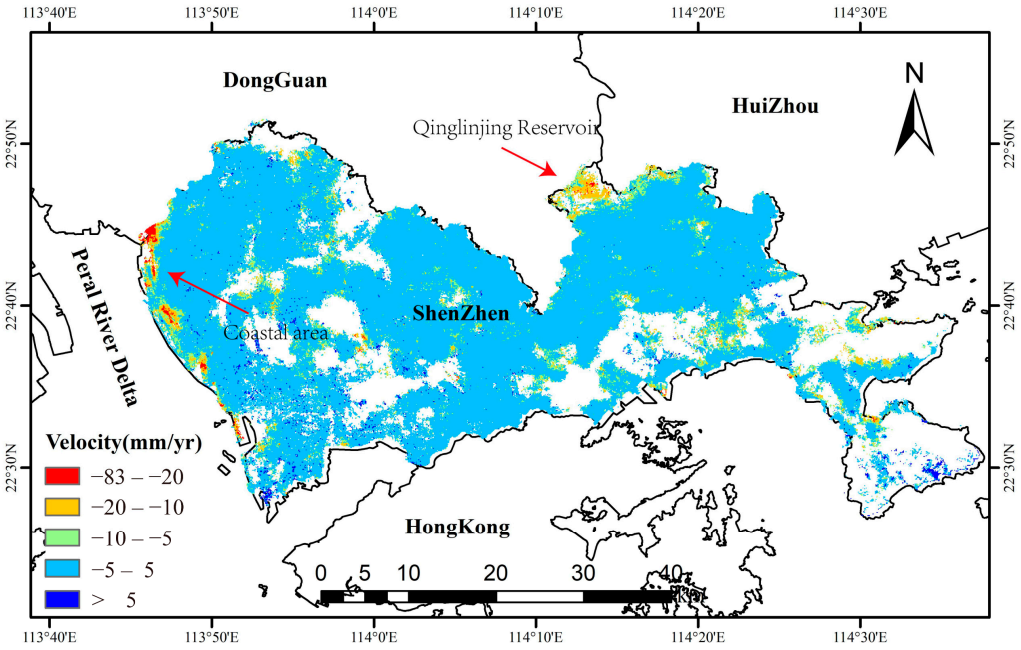

Figure 4. Subsidence rate map of the study area.

4.2. Reliable Subsidence Regions

Due to the high vegetation coverage in Shenzhen, we have appropriately lowered the submergence threshold to ensure a certain sampling rate (masking those below 0.4), which may increase the uncertainty of the results. This is a compromise technique in specific circumstances. Therefore, using the standard deviation (STD) as a reference, we artificially filter and extract the genuine subsidence regions. However, from the statistical histogram shown in Figure 5, it can be observed that the proportion of reliable subsidence ranges is not high (threshold divided by 1.5 times the STD).

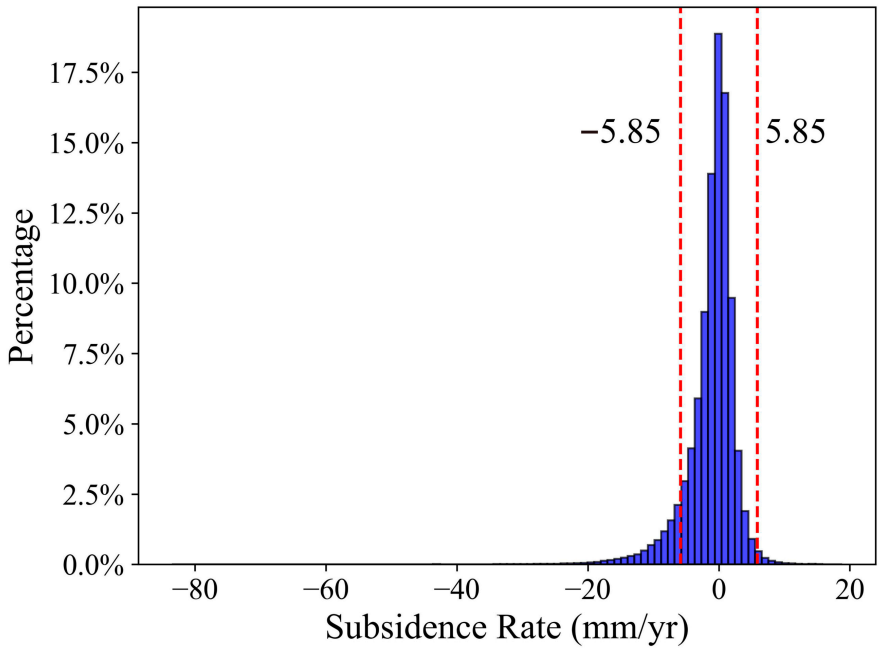

Figure 5. Subsidence rate distribution intervals.

The STD of the entire subsidence rate map is 3.9. Reliable subsidence regions were extracted based on ±1.5 times (5.85) the STD, in Figure 6, as within 1.5 times the STD is typically considered stable, while areas beyond this threshold are likely genuine subsidence regions [38,39]. It was observed that significant land subsidence is distributed in the coastal reclamation area on the western side of Bao'an District and in the reservoir area of Qinglinjing. Spatially, these findings are largely consistent with previous research results.

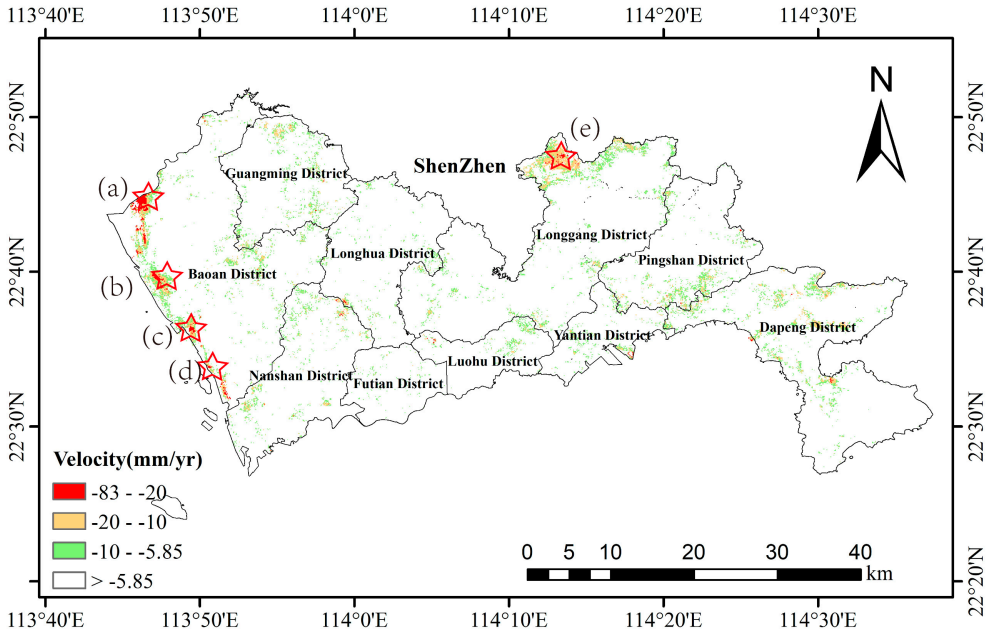

Figure 6. Land subsidence administrative division distribution. (a) Dongbao River estuary, (b) Shenzhen Bao'an international airport, (c) the construction site of the North Shenfen Expressway in the West Bay Coastal Park, (d) Dachan bay port, and (e) Qinglinjing reservoir.

5. Discussion

From the final subsidence results, it is evident that Shenzhen indeed experiences significant land subsidence, with spatial distribution being quite dispersed and the causes being rather complex. Through comparative analysis, it is observed that the land subsidence in Shenzhen can be broadly classified into three categories: subsidence in the reclamation areas, scattered construction-related subsidence within the city, and subsidence near the Qinglinjing Reservoir.

5.1. Land Subsidence in Reclamation Areas and Its Causal Analysis

Since 1979, the reclamation areas in Shenzhen are roughly as shown in Figure 7 [40]. However, with the rapid expansion of the city and the rapid growth of land demand, the scarcity of land resources in Shenzhen has become increasingly prominent. Reclamation has become one of the important ways for Shenzhen to alleviate land supply problems (the reclamation areas in Shenzhen are mainly distributed along the coastlines of Bao'an District, Nanshan District, and Futian District). Data shows that from 1990 to 2015 alone, Shenzhen reclaimed more than 80 km^2 of land. Reclamation areas are more prone to subsidence than ordinary land [41], which is an important prerequisite for land subsidence in this area.

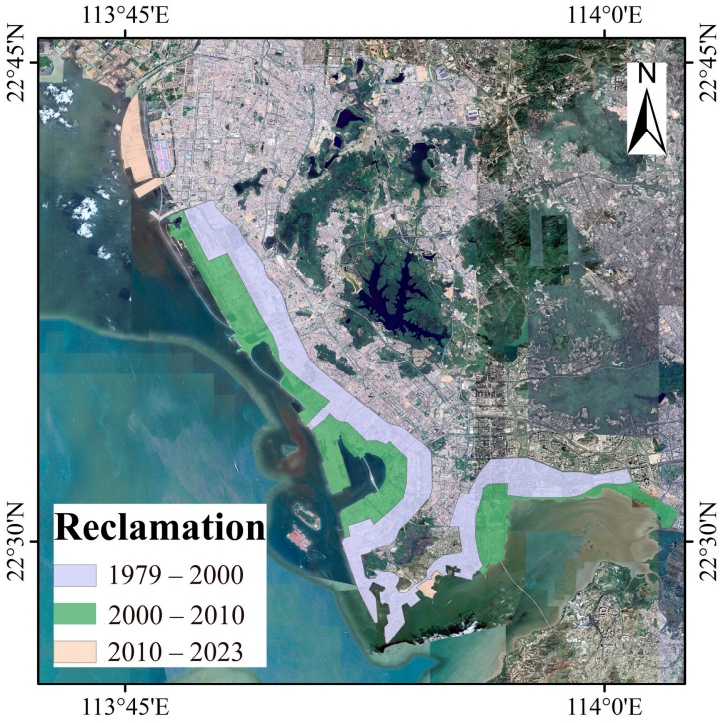

Figure 7. Reclamation areas since 1979, adapted from [40].

The analysis indicates the presence of multiple concentrated and contiguous severe subsidence areas in the western coastal region of Shenzhen. These severe subsidence areas are located at river estuaries or in the areas under construction for reclamation. These severe subsidence areas can be roughly categorized into four concentrated contiguous zones, distributed as indicated by the pentagram symbols in Figure 6. From north to south, they are the estuary of Dongbao River—Shenzhen International Convention and Exhibition Center, Shenzhen Bao'an International Airport, the construction site of Xiwandao Coastal Park and North Shenkeng Expressway, and the area above the Da Chan Bay Terminal, respectively. Further details are illustrated in Figure 8.

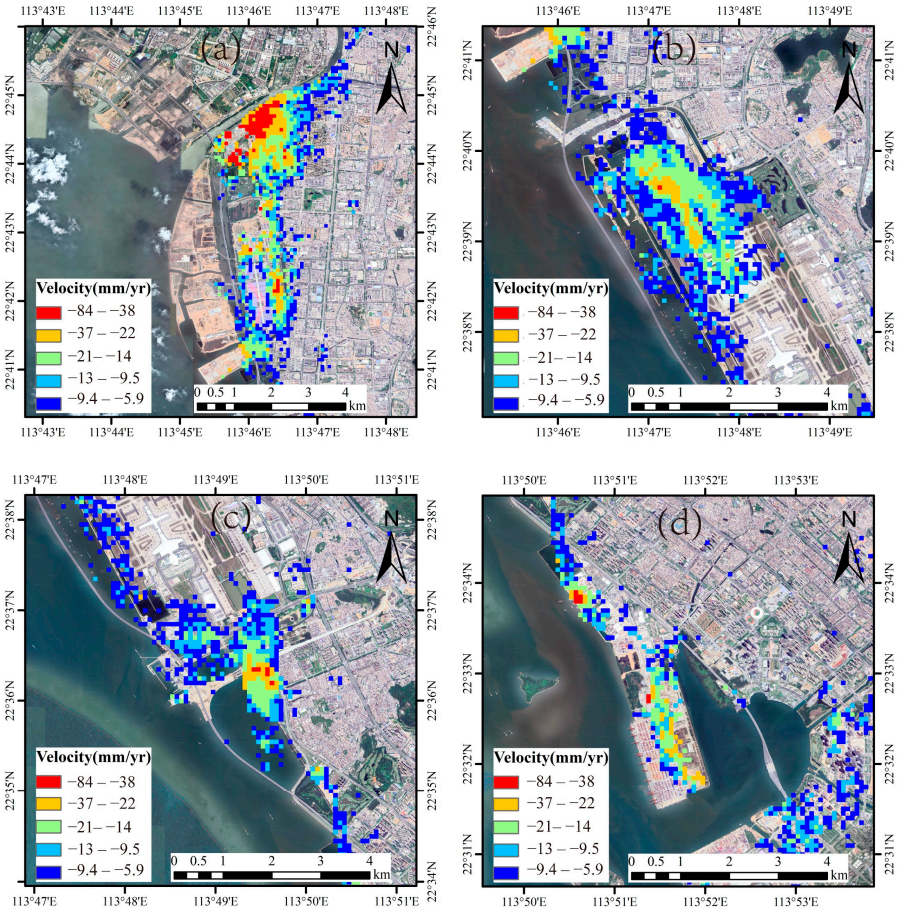

Figure 8. Significant subsidence centers along the coastal area of Bao'an District in western Shenzhen. (**a**) Dongbao River estuary, (**b**) Shenzhen Bao'an international airport, (**c**) the construction site of the North Shenfen Expressway in the West Bay Coastal Park, (**d**) Dachan bay port.

In the above areas, except for the Da Chan Bay Terminal which shows no apparent signs of construction, the other three locations are currently under construction. The subsidence time series for each pixel in these four subsidence areas are illustrated in Figure 9.

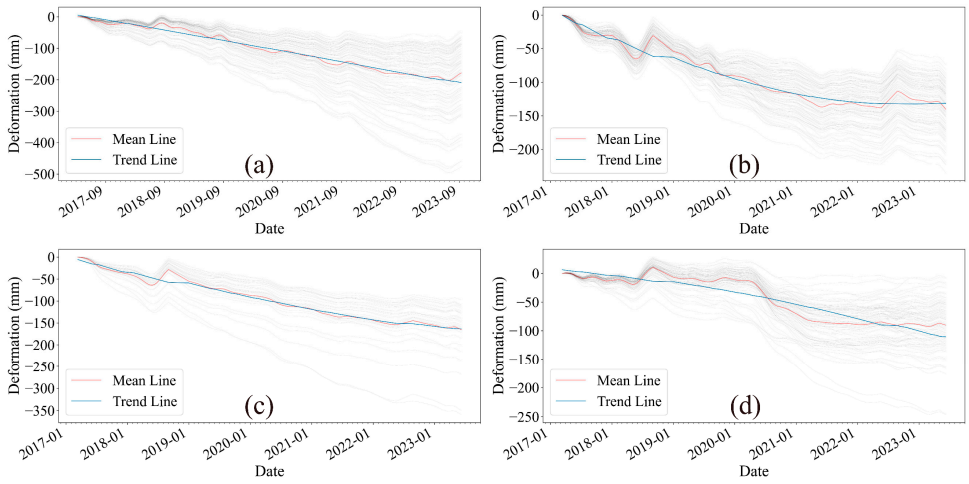

Figure 9. The subsidence time series corresponding to the subsidence centers with average values. (**a**) Subsidence time series of Dongbao River estuary, (**b**) Subsidence time series of Shenzhen Bao'an international airport, (**c**) Subsidence time series of the North Shenfen Expressway construction site in the West Bay Coastal Park, (**d**) Subsidence time series of Dachan bay port.

Region (a) is located in the coastal zone and comprises the Dongbao River estuary and the International Convention and Exhibition Center. The Dongbao River estuary area shows a stable and continuous subsidence trend. Investigation reveals that this area is currently under construction, with high-rise buildings being erected to the east and north of the International Convention and Exhibition Center. These buildings have reached their basic structural completion. The geological formation of this area consists mainly of soft river sediments, owing to its location at the river estuary. Such geological conditions predispose it to significant subsidence. Therefore, the subsidence in this area is most likely attributed to the excavation work during the initial phase and the subsequent structural stress from the buildings.

Region (b) is the Shenzhen Bao'an International Airport. Currently, based on the imagery, construction is observed on the northern side of the airport, resulting in significant land subsidence extending near the terminal building. Additionally, there is notable subsidence observed on the airport runway, which may be related to the significant impact of aircraft landings on the ground. Subsidence in this area started showing a noticeable deceleration trend around June 2021, indicating a stabilization of deformation.

Region (c) is the construction site of the North Shenfen Expressway in the West Bay Coastal Park. The land subsidence in this area is also relatively stable and continuous. Based on the imagery, it is evident that this area is a significant construction site and material stockpile area for the construction of the Shenfen Expressway. The analysis suggests that the land subsidence in this area is directly related to the stress from excavation pits and material stockpiles.

Region (d) corresponds to the Dachan Bay Port in Shenzhen. The subsidence process in the Da Chan Bay Port area is relatively complex. There was a significant acceleration of subsidence around May 2020, but it stabilized after June 2021. Since data on the volume of cargo stored in this area cannot be obtained, it is not possible to determine whether the change in land subsidence in this area is directly related to the amount of cargo stored. However, as this area is a port mainly used for container handling and storage, there may be a strong correlation between land subsidence and cargo stress. Additionally, this area was reclaimed from the sea, and the consolidation settlement of soil may take a long time. Therefore, it cannot be ruled out that long-term subsidence may continue to occur in this area in the future.

5.2. Construction-Related Subsidence

After filtering with 1.5 times the STD, visual interpretation revealed at least 45 different sizes of construction-related land subsidence throughout Shenzhen. Their distribution is shown in Figure 10.

It can be observed that large-scale urban construction projects such as urban surface construction and subway construction, as well as underground water extraction, are the main causes of land subsidence within the city and along subway and road corridors.

From the final subsidence rate map, during the monitoring period (from March 2017 to June 2023), except for the coastal areas and the vicinity of the Qinglinjing Reservoir, Shenzhen remained relatively stable overall. The few areas experiencing significant subsidence were mostly located in construction zones, with maximum subsidence reaching around 80 mm.

The influence of construction on land subsidence is closely related to groundwater level [29,42]. Excavation construction of foundation pits, whether using vertical excavation with support systems or "unprotected open cut excavation" will encounter the issue of groundwater impact on pit construction if the groundwater level in the construction area is high. When the excavation face is below the groundwater level, the water-bearing strata are severed, causing groundwater to continuously infiltrate into the pit from outside or the bottom. Additionally, rainfall or other factors during excavation may result in stagnant water in the pit, leading to a decrease in the strength of the foundation soil at the bottom.

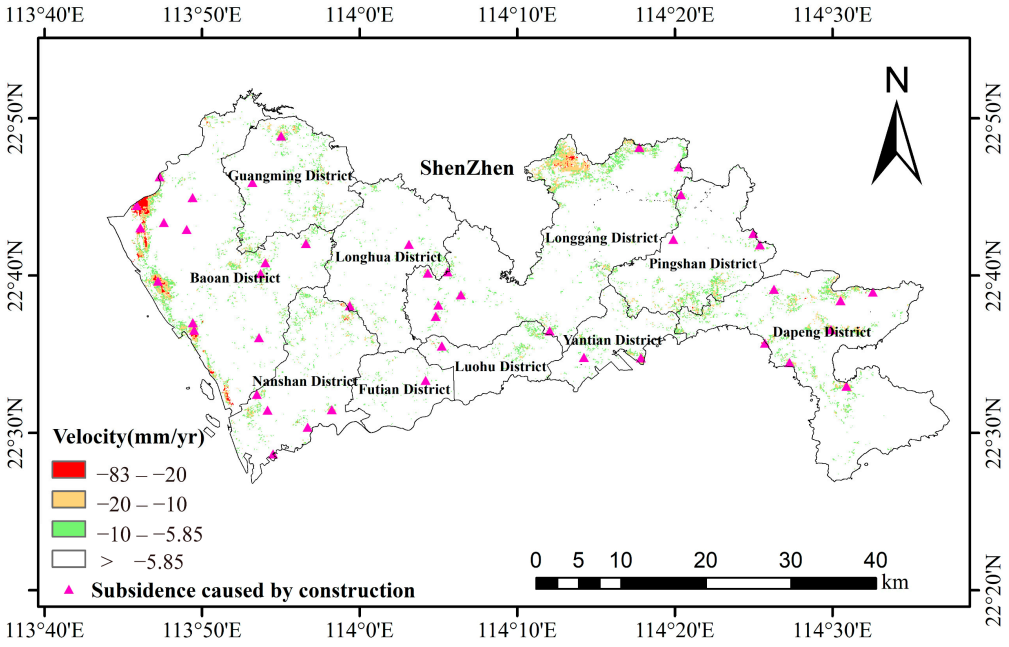

Figure 10. Visual interpretation was used to extract the distribution of subsidence caused by construction-related activities.

From a safety perspective in excavation construction, for vertical excavation with support systems, the increase in moisture content in the passive zone soil due to water infiltration leads to reduced strength and stiffness, which is detrimental to controlling the stability, strength, and deformation of the support system. For open cut excavation, it also increases the risk of slope instability and sand flow.

From a construction perspective, excavating below the groundwater level increases the difficulty of earthwork excavation and hinders the smooth progress of underground structure construction. Therefore, to ensure the smooth progress of deep foundation pit excavation construction and the normal progress of underground structure construction without compromising the strength of the foundation soil, measures to lower the groundwater level should be taken when the excavation face is below the groundwater level to keep the pit dry and facilitate construction.

Currently, lowering the groundwater level before excavation has been proven to be an important influencing factor on the deformation of retaining structures before excavation of foundation pits. Normal soil with water content will cause surface subsidence after precipitation, primarily due to changes in effective stress in the soil within the precipitation funnel during the precipitation process, resulting in compression of the soil, manifested as surface subsidence at a macro level.

5.3. Land Subsidence and Factor Analysis of Qinglinjing Reservoir

The annual precipitation in Shenzhen is approximately 1900 mm. Despite the abundant rainfall, it is difficult to retain atmospheric precipitation in this area due to insufficient surface runoff and limited utilization of groundwater. Consequently, this coastal city has relied on imported water since the 1960s, with water diverted from the Dongjiang River accounting for 80% of the total water consumption.

Although located along the coast, Shenzhen is also one of the severely water-scarce cities in China, with about 70% of its total water supply coming from external sources. There is a significant long-term water supply gap. Therefore, Shenzhen has planned and constructed three major water storage-regulation systems, centered around the Gongming Reservoir, Qinglinjing Reservoir, and the Songzikeng and Haiwan Reservoirs, to ensure the city's water supply security. The expansion project of the Qinglinjing Reservoir began in 2010, merging the original Qinglinjing Reservoir, Huanglong Lake Reservoir, and Bogongao

Reservoir into a large reservoir. It covers an area of 10.6 km^2, with a catchment area of 28.2 km^2. The normal water storage level is 79 m, and the total storage capacity reaches 1.86×10^8 m^3. The main dam of the reservoir is a homogeneous earth dam, and the expansion project was completed by the end of 2019.

Since its construction, the Qinglinjing Reservoir has been gradually filled with water through ongoing construction activities, causing the water level to rise year by year. Through MT-InSAR analysis, it has been observed that the phenomenon of land subsidence in this area is quite pronounced, such as Figure 11, despite the absence of any apparent ongoing construction. Additionally, due to the construction of the reservoir, a large number of indigenous people have been relocated, resulting in a significant reduction in human activity in the area. Furthermore, recent analysis of optical imagery has not revealed any other significant signs of human construction activity. Therefore, after ruling out these two possibilities, it is believed that the cause of land subsidence in this area originates from the excessive land stress resulting from reservoir water storage.

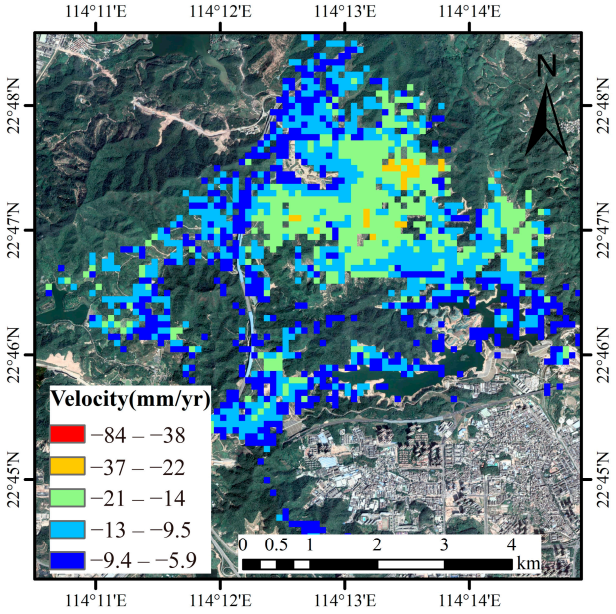

Figure 11. Current status of subsidence rate at Qinglinjing Reservoir.

Furthermore, from the subsidence time series shown in Figure 12, the land subsidence process of the Qinglinjing Reservoir exhibits significant seasonal fluctuations, and overall subsidence shows a trend of gradual deceleration. Seasonal fluctuations occur, with a noticeable fluctuation every September which may be related water storage, watershed runoff, and seasonal peak water demand in September.

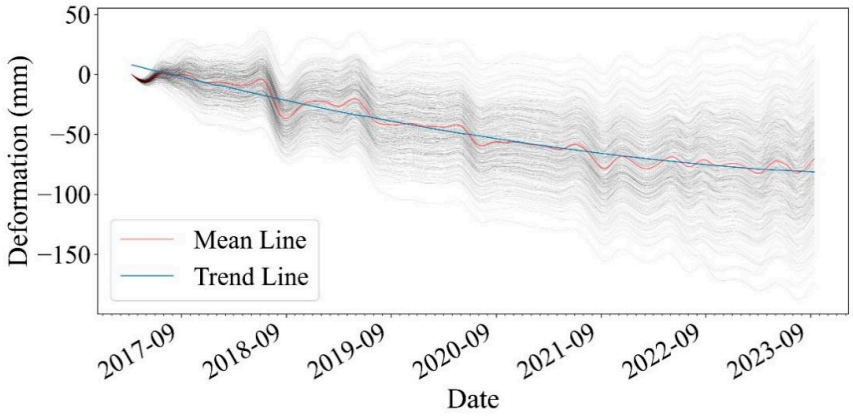

Figure 12. Subsidence time series of Qinglinjing Reservoir reservoir area.

Current reports on reservoir-induced earthquakes are not uncommon, with nearly 40 reservoir-induced earthquakes reported [43], such as those at the Xinfengjiang Reservoir [43], the Three Gorges [44,45], and Xiluodu Reservoir [46]. The main cause of reservoir-induced earthquakes is the fragile bottom layer facing increasing gravitational potential energy. Therefore, it is necessary to strengthen the subsidence monitoring of the Qinglinjing Reservoir in the future to prevent destructive geological disasters such as dam cracks from occurring.

5.4. Destructive Impacts of Land Subsidence and Countermeasures

Rainfall is a norm during the summer and autumn in Shenzhen, where flood, waterlogging, and tidal (storm surge) disasters are extremely frequent. In such a context, land subsidence in Shenzhen undoubtedly exacerbates the risk and destructiveness of flood, waterlogging, and tidal disasters.

(1) Urban and Coastal Flooding

Shenzhen experiences a humid climate during the summer season, characterized by significant rainfall, especially during the monsoon season. Rainfall events can trigger urban flooding, particularly in low-lying areas within the city. Additionally, Shenzhen is annually affected by typhoons originating from the Pacific Ocean. Typhoons typically bring strong winds and heavy rainfall, further increasing the likelihood of flooding events.

As shown in Figure 13 topographic map, the coastal areas of western Bao'an District are relatively low-lying and vulnerable to threats from rising sea levels and storm surges. While some inland areas have relatively higher elevations, certain areas are surrounded by mountains, forming localized basin topography, which hinders the drainage of rainfall. Moreover, the high degree of urbanization in the city has resulted in extensive impermeable surfaces, impeding rapid rainwater infiltration and consequently increasing flood risks.

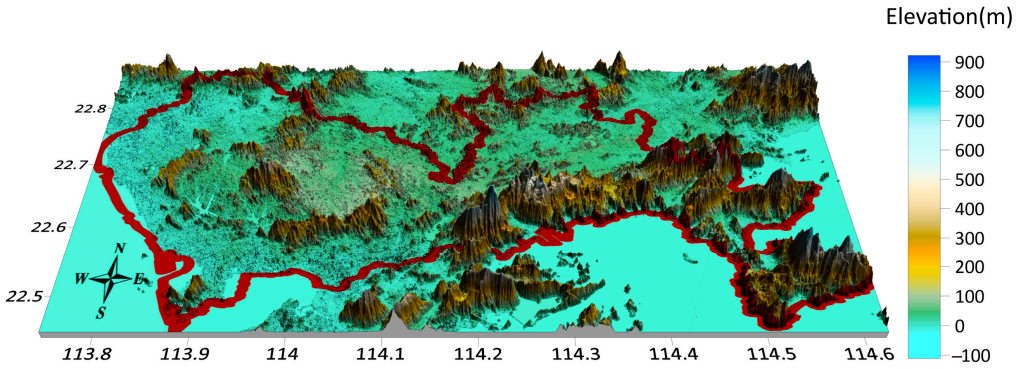

Figure 13. Shenzhen Topography.

Currently, there is no evidence of widespread concentrated land subsidence in the inland areas of Shenzhen, indicating that land subsidence has not significantly impacted flood risk in these regions. However, the land subsidence in coastal areas cannot be overlooked.

(2) Port Terminals and Hydraulic Protection Facilities

Port terminals are integral to Shenzhen's infrastructure. Land subsidence may have a range of effects on port terminals. Land subsidence may lead to instability in the structures of port terminals, increasing structural loads and potentially causing issues such as cracking, tilting, or collapse. Port equipment and facilities are typically installed at designed elevations. If land subsidence occurs, these facilities may be damaged, affecting the normal operation of the port. Land subsidence may require port management to allocate more resources for maintenance and repair to ensure the sustainable operation of port facilities.

5.5. Limitation of This Study

In this study, we employed MT-InSAR technology to conduct a detailed investigation and analysis of the land subsidence phenomenon in Shenzhen. Nonetheless, several limita-

tions should be acknowledged. Despite high precision and expansive coverage, it remains susceptible to factors such as atmospheric interference, ground cover, radar geometry, and angular resolution. These elements have the potential to introduce inaccuracies or incomplete subsidence data in certain regions. To ameliorate the impact of these constraints on our findings, future investigations may integrate additional geological survey methodologies, including leveling and GPS monitoring, to acquire more precise and comprehensive land subsidence data.

Moreover, our study did not encompass all areas of Shenzhen. The nature of land subsidence can vary significantly across different regions, particularly in those with intricate geological conditions. Consequently, expanding our research scope to cover the entirety of Shenzhen, and even adjacent geologically sensitive zones, would facilitate a more profound comprehension of the distribution and influencing factors of land subsidence.

Concerning data analysis, our primary focus was on the rate and extent of land subsidence, while the underlying mechanisms and causes received less quantitative attention. Future studies would benefit from a deeper exploration of the quantitative correlation between land subsidence and driving factors such as groundwater extraction, geological structure, soil type, and others. This approach would provide a stronger scientific foundation for preventing and managing ground subsidence. Although our study offers valuable insights into the land subsidence issues in Shenzhen, numerous limitations still exist. By addressing these limitations and situating them within a broader research framework, we can foster a more holistic understanding of land subsidence and devise more effective prevention and management strategies.

6. Conclusions

This study conducted an analysis of land subsidence across the entire city of Shenzhen using MT-InSAR technology. The findings indicate several notable areas of land subsidence in the Shenzhen region. Combining the analysis with optical imagery, it was discovered that the causes of land subsidence in Shenzhen are complex, and the phenomenon is expected to undergo changes over the coming period based on human activities. The current research on land subsidence in Shenzhen reveals the following: (1) Land subsidence in the western coastal zone of Shenzhen exhibits notable concentration and considerable magnitude, with rates exceeding 80 mm/yr in certain areas. This phenomenon primarily stems from the subsidence of unstable geological strata in reclamation zones, exacerbated by human activities such as excessive loading and fluctuations in water levels; (2) Apart from the pronounced and concentrated subsidence along the coastline of Bao'an District, the spatial distribution of land subsidence primarily manifests as scattered instances of construction subsidence. Based on deformation trends, most instances of construction subsidence are expected to persist for a finite duration, with a gradual deceleration in the rate of change over time; (3) The land subsidence observed at the Qinglinjing Reservoir may be attributed to factors such as the reservoir's water storage volume and the geological characteristics of its location. Given the findings of prior research on reservoir-induced seismicity, it is advisable to enhance monitoring efforts for land subsidence in this area in the future.

Newly subsiding areas require timely attention and prevention measures. Areas experiencing aggravated subsidence require positive intervention measures. Moreover, no new surface or underground constructions should be added around these areas. Unstable surface areas are unsuitable for constructing tall buildings, large structures, or transportation infrastructure with high precision requirements. Attention should also be paid to changes in groundwater levels in these areas. Continuous monitoring is necessary for areas experiencing ongoing subsidence to constantly track their dynamic changes.

Author Contributions: Conceptualization, S.W. and G.W.; methodology, S.W. and G.W.; validation, S.W. and G.W.; formal analysis, S.W. and G.W.; investigation, S.W., G.W., M.H., J.S., X.Y., T.Z., S.Z., W.W., C.W. and J.X.; resources, S.W., G.W., M.H., J.S., X.Y., T.Z., S.Z., W.W., C.W. and J.X.; writing—original draft preparation, S.W. and G.W.; writing—review & editing, S.W., G.W. and W.J.; project

administration, S.W.; data curation, S.W. and G.W.; visualization, S.W. and G.W.; supervision, G.W.; funding acquisition, S.W. All authors have read and agreed to the published version of the manuscript.

Funding: This study was supported by the Research and development of high-precision shipborne lasers canning coastal dynamic monitoring system. (No. 201507201828399050).

Data Availability Statement: The original contributions presented in the study are included in the article, further inquiries can be directed to the corresponding author.

Acknowledgments: The authors are grateful for all of the open source datasets. The Sentinel-1 and Landsat-8 data used in this study are freely available from ESA and the USGS. The SRTM data products distributed by NASA's Land Processes Distributed Active Archive Center (LP DAAC) are freely available. Google Earth images are used to describe the location of study area.

Conflicts of Interest: Author ShuanglongWang was employed by the company "Shenzhen Intergrated Geotechnical Investigation & Surveying Co., Ltd.". The remaining authors declare that the research was conducted in the absence of any commercial or financial relationships that could be construed as a potential conflict of interest.

References

1. Kulp, S.A.; Strauss, B.H. New elevation data triple estimates of global vulnerability to sea-level rise and coastal flooding. *Nat. Commun.* **2019**, *10*, 4844. [CrossRef]
2. Cazenave, A.; Cozannet, G.L. Sea level rise and its coastal impacts. *Earth's Future* **2014**, *2*, 15–34. [CrossRef]
3. Williams, S.J. Sea-Level Rise Implications for Coastal Regions. *J. Coast. Res.* **2013**, *63*, 184–196. [CrossRef]
4. Allison, M.; Yuill, B.; Törnqvist, T.; Amelung, F.; Dixon, T.; Erkens, G.; Stuurman, R.; Jones, C.; Milne, G.; Steckler, M.; et al. Global risks and research priorities for coastal subsidence. *Eos Trans. Am. Geophys. Union* **2016**, *97*, 22–27. [CrossRef]
5. Chini, M.; Pulvirenti, L.; Pierdicca, N. Analysis and Interpretation of the COSMO-SkyMed Observations of the 2011 Japan Tsunami. *IEEE Geosci. Remote Sens. Lett.* **2012**, *9*, 467–471. [CrossRef]
6. Nicholls, R.J.; Cazenave, A. Sea-Level Rise and Its Impact on Coastal Zones. *Science* **2010**, *328*, 1517–1520. [CrossRef] [PubMed]
7. Nicholls, R.J.; Lincke, D.; Hinkel, J.; Brown, S.; Vafeidis, A.T.; Meyssignac, B.; Hanson, S.E.; Merkens, J.-L.; Fang, J. A global analysis of subsidence, relative sea-level change and coastal flood exposure. *Nat. Clim. Chang.* **2021**, *11*, 338–342. [CrossRef]
8. Wang, G.; Li, P.; Li, Z.; Ding, D.; Qiao, L.; Xu, J.; Li, G.; Wang, H. Coastal Dam Inundation Assessment for the Yellow River Delta: Measurements, Analysis and Scenario. *Remote Sens.* **2020**, *12*, 3658. [CrossRef]
9. Gracia, V.; Sierra, J.P.; Gómez, M.; Pedrol, M.; Sampé, S.; García-León, M.; Gironella, X. Assessing the impact of sea level rise on port operability using LiDAR-derived digital elevation models. *Remote Sens. Environ.* **2019**, *232*, 111318. [CrossRef]
10. Gebremichael, E.; Sultan, M.; Becker, R.; El Bastawesy, M.; Cherif, O.; Emil, M. Assessing Land Deformation and Sea Encroachment in the Nile Delta: A Radar Interferometric and Inundation Modeling Approach. *J. Geophys. Res. Solid Earth* **2018**, *123*, 3208–3224. [CrossRef]
11. Syvitski, J.P.M.; Kettner, A.J.; Overeem, I.; Hutton, E.W.H.; Hannon, M.T.; Brakenridge, G.R.; Day, J.; Vorosmarty, C.; Saito, Y.; Giosan, L.; et al. Sinking Deltas due to Human Activities. *Nat. Geosci.* **2009**, *2*, 681–686. [CrossRef]
12. Shirzaei, M.; Bürgmann, R. Global climate change and local land subsidence exacerbate inundation risk to the San Francisco Bay Area. *Sci. Adv.* **2018**, *4*, eaap9234. [CrossRef]
13. Yin, J.; Zhao, Q.; Yu, D.; Lin, N.; Kubanek, J.; Ma, G.; Liu, M.; Pepe, A. Long-term flood-hazard modeling for coastal areas using InSAR measurements and a hydrodynamic model: The case study of Lingang New City, Shanghai. *J Hydrol.* **2019**, *571*, 593–604. [CrossRef]
14. Syvitski, J.; Ángel, J.R.; Saito, Y.; Overeem, I.; Vörösmarty, C.J.; Wang, H.; Olago, D. Earth's sediment cycle during the Anthropocene. *Nat. Rev. Earth Environ.* **2022**, *3*, 179–196. [CrossRef]
15. Herrera-García, G.; Ezquerro, P.; Tomás, R.; Béjar-Pizarro, M.; López-Vinielles, J.; Rossi, M.; Mateos, R.M.; Carreón-Freyre, D.; Lambert, J.; Teatini, P.; et al. Mapping the global threat of land subsidence. *Science* **2021**, *371*, 34–36. [CrossRef] [PubMed]
16. Li, P.; Wang, G.; Liang, C.; Wang, H.; Li, Z. InSAR-derived Coastal Subsidence Reveals New Inundation Scenarios over the Yellow River Delta. *IEEE J. Sel. Top. Appl. Earth Obs. Remote Sens.* **2023**, *16*, 8431–8441. [CrossRef]
17. Hallegatte, S.; Green, C.; Nicholls, R.J.; Corfee-Morlot, J. Future flood losses in major coastal cities. *Nat. Clim. Chang.* **2013**, *3*, 802–806. [CrossRef]
18. Zhu, B.; Chu, Z.; Shen, F.; Tang, W.; Wang, B.; Wang, X. Land subsidence (2004–2013) in Changzhou in Central Yangtze River delta revealed by MT-InSAR. *Nat. Hazards* **2019**, *97*, 379–394. [CrossRef]
19. Wang, G.; Li, P.; Li, Z.; Liang, C.; Wang, H. Coastal subsidence detection and characterization caused by brine mining over the Yellow River Delta using time series InSAR and PCA. *Int. J. Appl. Earth Obs. Geoinf.* **2022**, *114*, 103077. [CrossRef]
20. Wang, G.; Li, P.; Li, Z.; Liu, J.; Zhang, Y.; Wang, H. InSAR and machine learning reveal new understanding of coastal subsidence risk in the Yellow River Delta, China. *Sci. Total Environ.* **2024**, *915*, 170203. [CrossRef]
21. Liu, Y.; Liu, J.; Xia, X.; Bi, H.; Huang, H.; Ding, R.; Zhao, L. Land subsidence of the Yellow River Delta in China driven by river sediment compaction. *Sci. Total Environ.* **2021**, *750*, 142165. [CrossRef]

22. Wang, H.; Wright, T.J.; Yu, Y.; Lin, H.; Jiang, L.; Li, C.; Qiu, G. InSAR reveals coastal subsidence in the Pearl River Delta, China. *Geophys. J. Int.* **2012**, *191*, 1119–1128. [CrossRef]
23. Qiang, Y.J.; Zhang, L.M.; He, J.; Xiao, T.; Huang, H.H.; Wang, H.J. Urban flood analysis for Pearl River Delta cities using an equivalent drainage method upon combined rainfall-high tide-storm surge events. *J. Hydrol.* **2021**, *597*, 126293. [CrossRef]
24. Su, G.; Wu, Y.; Zhan, W.; Zheng, Z.; Chang, L.; Wang, J. Spatiotemporal evolution characteristics of land subsidence caused by groundwater depletion in the North China plain during the past six decades. *J. Hydrol.* **2021**, *600*, 126678. [CrossRef]
25. Li, M.; Ge, D.; Zhang, L.; Guo, X.; Liu, B.; Wang, Y.; Wu, Q. Assessment of the temporal–spatial evolution of subsidence and its driving mechanism in the Beijing Plain (China) by using SAR interferometry and geological data. *Geomat. Nat. Hazards Risk* **2021**, *12*, 2708–2735. [CrossRef]
26. Xu, B.; Feng, G.; Li, Z.; Wang, Q.; Wang, C.; Xie, R. Coastal Subsidence Monitoring Associated with Land Reclamation Using the Point Target Based SBAS-InSAR Method: A Case Study of Shenzhen, China. *Remote Sens.* **2016**, *8*, 652. [CrossRef]
27. Du, Y.; Feng, G.; Li, Z.; Peng, X.; Zhu, J.; Ren, Z. Effects of External Digital Elevation Model Inaccuracy on StaMPS-PS Processing: A Case Study in Shenzhen, China. *Remote Sens.* **2017**, *9*, 1115. [CrossRef]
28. Liu, P.; Chen, X.; Li, Z.; Zhang, Z.; Xu, J.; Feng, W.; Wang, C.; Hu, Z.; Tu, W.; Li, H. Resolving Surface Displacements in Shenzhen of China from Time Series InSAR. *Remote Sens.* **2018**, *10*, 1162. [CrossRef]
29. Sun, M.; Du, Y.A.; Liu, Q.Y.; Feng, G.C.; Peng, X.; Liao, C.H. Understanding the Spatial-Temporal Characteristics of Land Subsidence in Shenzhen under Rapid Urbanization Based on MT-InSAR. *IEEE J. Sel. Top. Appl. Earth Obs. Remote Sens.* **2023**, *16*, 4153–4166. [CrossRef]
30. Zhou, L.; Liu, S.G.; Li, J.H.; Pan, Y.J.; Wang, C.; Huang, L.K.; Huang, L. Investigating Surface Deformation and Its Intrinsic Mechanism in Shenzhen, China Using Sentinel-1A SAR Imagery. *Earth Space Sci.* **2023**, *10*, e2023EA002905. [CrossRef]
31. Yu, G.M.; Xia, P.J.; Zhang, Y.Y.; Shi, Q.M.; Jun, L.; Song, P.F.; Tan, Z.W.; Hao, L.; Ze, C. Land Lapse Phenomenon and Surface Subsidence Law of Shield Tunnel Passing through Rock-Bearing Formation. *Front. Earth Sci.* **2022**, *10*, 934360. [CrossRef]
32. He, Y.F.; Xu, G.C.; Kaufmann, H.; Wang, J.T.; Ma, H.; Liu, T. Integration of InSAR and LiDAR Technologies for a Detailed Urban Subsidence and Hazard Assessment in Shenzhen, China. *Remote Sens.* **2021**, *13*, 2366. [CrossRef]
33. Liang, H.Y.; Zhang, L.; Li, X. Enhancing MTInSAR Phase Unwrapping in Decorrelating Environments by Spatiotemporal Observation Optimization. *IEEE Geosci. Remote Sens. Lett.* **2023**, *20*, 4002505. [CrossRef]
34. Wu, W.Q.; Cui, H.T.; Hu, J.; Yao, L.N. Detection and 3D Visualization of Deformations for High-Rise Buildings in Shenzhen, China from High-Resolution TerraSAR-X Datasets. *Appl. Sci.* **2019**, *9*, 3818. [CrossRef]
35. Ding, J.Z.; Zhao, Q.; Tang, M.C.; Calò, F.; Zamparelli, V.; Falabella, F.; Liu, M.; Pepe, A. On the Characterization and Forecasting of Ground Displacements of Ocean-Reclaimed Lands. *Remote Sens.* **2020**, *12*, 2971. [CrossRef]
36. Berardino, P.; Fornaro, G.; Lanari, R.; Sansosti, E. A new algorithm for surface deformation monitoring based on small baseline differential SAR interferograms. *IEEE Trans. Geosci. Remote Sens.* **2002**, *40*, 2375–2383. [CrossRef]
37. Ge, D.Q.; Zhang, L.; Wang, Y.; Guo, X.F.; Xia, Y. Merging Multi-Track Psi Result for Land Subsidence Mapping over Very Extended Area. In Proceedings of the 2010 IEEE International Geoscience and Remote Sensing Symposium, Honolulu, HI, USA, 25–30 July 2010; pp. 3522–3525.
38. Fernández-Torres, E.A.; Cabral-Cano, E.; Solano-Rojas, D.; Salazar-Tlaczani, L.; Gárcia-Venegas, J.; Marquez-Azúa, B.; Graham, S.; Villarnobo-Gonzalez, K.M. Country-scale assessment of urban areas, population, and households exposed to land subsidence using Sentinel-1 InSAR, and GPS time series. *Nat. Hazards* **2024**, *120*, 1577–1601. [CrossRef]
39. Tomás, R.; Pagán, J.I.; Navarro, J.A.; Cano, M.; Pastor, J.L.; Riquelme, A.; Cuevas-González, M.; Crosetto, M.; Barra, A.; Monserrat, O.; et al. Semi-Automatic Identification and Pre-Screening of Geological–Geotechnical Deformational Processes Using Persistent Scatterer Interferometry Datasets. *Remote Sens.* **2019**, *11*, 1675. [CrossRef]
40. Zhou, L.; Shi, X.; Ren, C.; Huang, Y.; Zhu, Z. Monitoring and Analysis of Land Subsidence in Shenzhen reclamation area Based on Sentinel-1A Interferometric Synthetic Aperture Radar. *Sci. Technol. Eng.* **2021**, *21*, 8765–8769.
41. Li, D.; Li, B.; Zhang, Y.; Fan, C.; Xu, H.; Hou, X. Spatial and temporal characteristics analysis for land subsidence in Shanghai coastal reclamation area using PS-InSAR method. *Front. Mar. Sci.* **2022**, *9*, 1000523. [CrossRef]
42. Xu, Y.-S.; Wu, H.-N.; Wang, B.Z.-F.; Yang, T.-L. Dewatering induced subsidence during excavation in a Shanghai soft deposit. *Environ. Earth Sci.* **2017**, *76*, 351. [CrossRef]
43. Chang, T.G.; Li, B.H.; Zeng, X.X. Prediction and verification of earthquakes induced by the Xiluodu hydropower station reservoir. *Earthq. Sci.* **2022**, *35*, 387–397. [CrossRef]
44. Zhang, L.F.; Gahalaut, K.; Liao, W.L.; Zhao, Y.N.; Yao, Y.S.; Li, J.G.; Qin, W.B.; Wei, G.C.; Zhou, Z.Y. Application of spectral analysis to the reservoir-triggered earthquakes in Three Gorges reservoir region, China. *Nat. Hazards* **2023**, *118*, 479–494. [CrossRef]
45. Zhang, L.; Li, J.; Sun, X.; Liao, W.; Zhao, Y.; Wei, G.; He, C. A Possible Mechanism of Reservoir-Induced Earthquakes in the Three Gorges Reservoir, Central China. *Bull. Seismol. Soc. Am.* **2018**, *108*, 3016–3028. [CrossRef]
46. Lei, H.F.; Wang, Q.C.; Zhao, C.P.; Zhao, C.; Zhang, J.C.; Li, J. Seismic analysis of the Xiluodu reservoir area and insights into the geometry of seismogenic faults. *Earthq. Sci.* **2022**, *35*, 371–386. [CrossRef]